Rate Coefficients for the OH + HC(O)C(O)H (Glyoxal) Reaction between 210 and 390 K

Karl J. Feierabend,[†,‡] Lei Zhu,[†,‡] R. K. Talukdar,[†,‡] and James B. Burkholder*[,†]

Earth System Research Laboratory, Chemical Sciences Division, National Oceanic and Atmospheric Administration, 325 Broadway, Boulder, Colorado 80305-3328, and Cooperative Institute for Research in Environmental Sciences, University of Colorado, Boulder, Colorado 80309

Received: August 27, 2007; In Final Form: October 9, 2007

Rate coefficients, $k_1(T)$, over the temperature range of 210−390 K are reported for the gas-phase reaction OH + HC(O)C(O)H (glyoxal) → products at pressures between 45 and 300 Torr (He, N_2). Rate coefficients were determined under pseudo-first-order conditions in OH using pulsed laser photolysis production of OH radicals coupled with OH detection by laser-induced fluorescence. The rate coefficients obtained were independent of pressure and bath gas. The room-temperature rate coefficient, k_1(296 K), was determined to be $(9.15 \pm 0.8) \times 10^{-12}$ cm^3 molecule^{-1} s^{-1}. $k_1(T)$ shows a negative temperature dependence with a slight deviation from Arrhenius behavior that is reproduced over the temperature range included in this study by $k_1(T) = [(6.6 \pm 0.6) \times 10^{-18}]T^2[\exp([820 \pm 30]/T)]$ cm^3 molecule^{-1} s^{-1}. For atmospheric modeling purposes, a fit to an Arrhenius expression over the temperature range included in this study that is most relevant to the atmosphere, 210−296 K, yields $k_1(T) = (2.8 \pm 0.7) \times 10^{-12} \exp[(340 \pm 50)/T]$ cm^3 molecule^{-1} s^{-1} and reproduces the rate coefficient data very well. The quoted uncertainties in $k_1(T)$ are at the 95% confidence level (2σ) and include estimated systematic errors. Comparison of the present results with the single previous determination of k_1(296 K) and a discussion of the reaction mechanism and non-Arrhenius temperature dependence are presented.

1. Introduction

Glyoxal, HC(O)C(O)H, the simplest α-dicarbonyl, is a stable end-product formed in the atmospheric oxidation of a number biogenic and anthropogenic volatile organic compounds (VOCs), including isoprene[1] and terpenoids.[2−5] Satellite-based measurements of glyoxal in the atmosphere suggest that the oxidation of biogenic VOCs in tropical regions is an important source of glyoxal globally.[6] Glyoxal serves as a marker for "hot spots" of atmospheric organic chemistry, in part because it is a significant oxidation product of a variety of organic compounds.[6,7] The atmospheric processing of glyoxal also represents a significant source of HO_x (HO_x = OH + HO_2),[8] and it has been suggested that glyoxal may play a role in secondary organic aerosol (SOA) formation.[9−11]

The atmospheric lifetime of glyoxal is relatively short, on the order of hours, and is primarily determined by its reaction with the OH radical[7,8,12]

$$\mathrm{OH + HC(O)C(O)H \rightarrow HC(O)CO + H_2O} \qquad (1)$$

and by UV photolysis[13]

$$\mathrm{HC(O)C(O)H} + h\nu \rightarrow \text{products} \qquad (2)$$

Deposition, uptake onto existing aerosol (SOA formation), and gas-phase reaction with the NO_3 radical are additional possible loss processes for glyoxal. Despite the atmospheric importance of glyoxal and its molecular simplicity, only one experimental determination of the rate coefficient for reaction 1, k_1, has been reported in the literature to date; Plum et al.[12] used a relative rate method and reported k_1(296 K) = $(1.06 \pm 0.4) \times 10^{-11}$ cm^3 molecule^{-1} s^{-1}. This k_1(296 K) value is in poor agreement with the rate coefficient estimated using the structure−activity relationships (SAR) developed by Kwok and Atkinson,[14] 2.5×10^{-11} cm^3 molecule^{-1} s^{-1}. The JPL[15] and IUPAC[16] kinetic data evaluations currently recommend the rate coefficient reported by Plum et al. but include large estimated uncertainties, f(298 K) = 1.5 and $\Delta\log(k_1) = 0.4$, respectively, due to the lack of corroborative data. There are presently no published experimental rate coefficient data for the temperature dependence of k_1. The limited number of kinetic studies, the discrepancy with the SAR-estimated rate coefficient, and the absence of temperature-dependent data for reaction 1 motivated the present rate coefficient study.

Gas-phase reactions of OH with aldehydes have been shown to occur almost exclusively via H atom abstraction from the aldehydic group.[17−19] However, despite numerous laboratory measurements and theoretical studies, the details of the reaction mechanisms are at present not completely understood. A number of the OH + aldehyde reactions exhibit non-Arrhenius behavior and a negative temperature dependence, suggesting the formation of a stable prereactive adduct.[20] In addition, theoretical studies, such as those for the reactions of formaldehyde, HC(O)H, and acetaldehyde, $CH_3C(O)H$, with OH,[21,22] have provided evidence for an OH adduct as a reaction intermediate. Glyoxal is a small organic molecule and therefore suitable for relatively high levels of theoretical treatment. Galano et al.[23] have studied the reactions of OH with glyoxal and methylglyoxal, $CH_3C(O)C(O)H$, theoretically using ab initio quantum chemical structure (BHandHLYP/6-311++G(d,p)) and energy (CCSD(T)/6-311++G(d,p)) calculations combined with canonical variational transition state theory. They report a reaction

* To whom correspondence should be addressed. E-mail: James.B.Burkholder@noaa.gov.
† National Oceanic and Atmospheric Administration.
‡ University of Colorado.

10.1021/jp0768571 CCC: $40.75
Published on Web 12/01/2007

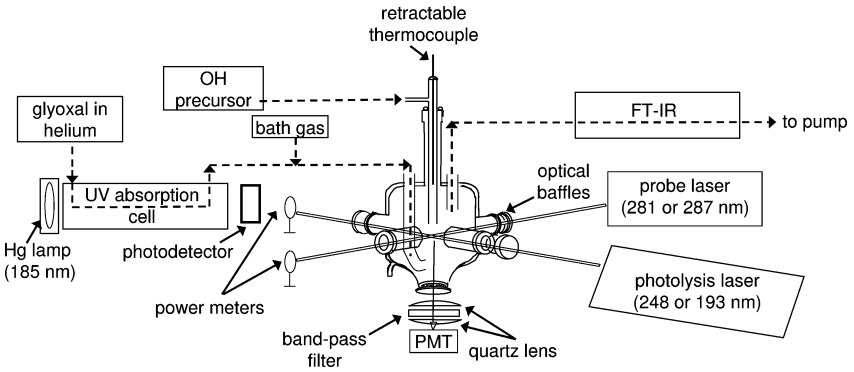

Figure 1. Schematic of the pulsed laser photolysis−laser-induced fluorescence (PLP−LIF) apparatus used to measure the rate coefficient for reaction 1, $k_1(T)$, OH + glyoxal → products. The dashed lines and arrows show the direction of the gas flow through the apparatus. Two OH radical precursors were used: H_2O_2 or a mixture of N_2O and CH_4 in a He bath gas. FT-IR = Fourier transform infrared spectrometer; PMT = photomultiplier tube.

mechanism that involves a weakly stabilized (<3 kcal mol^{-1}) OH−glyoxal adduct. The calculated k_1(296 K) is in reasonable agreement with the available experimental data but a factor of 2 smaller (the agreement for the OH + methylglyoxal reaction rate coefficient is much better). In addition, a negative temperature dependence for $k_1(T)$ was calculated with a slight deviation from Arrhenius behavior. Accurate experimental data for $k_1(T)$ over a wide temperature range will provide the information needed to validate and/or improve the theoretical methodology for this reaction.

In this paper, we report measurements of $k_1(T)$ over the temperature range of 210−390 K using the pulsed laser photolysis−laser-induced fluorescence (PLP−LIF) technique. Our results are compared with previously reported OH rate coefficient data for reaction 1 and several other small carbonyl compound reactions as well as rate coefficients estimated using the structure−activity relationships of Kwok and Atkinson.[14] The mechanism for reaction 1 is discussed in light of the recent theoretical study.[23] The significance of our rate coefficient measurements with regard to the role of glyoxal as an atmospheric source of HO_x is also discussed.

2. Experimental Section

Pulsed laser photolysis production of OH radicals coupled with its detection by laser-induced fluorescence (PLP−LIF) was used in the determination of the rate coefficient for reaction 1, $k_1(T)$, under pseudo-first-order conditions in OH, [OH] ≪ [HCOCOH]. The PLP−LIF apparatus is shown in Figure 1 and has been described in a recent study from this laboratory.[24] Therefore, the apparatus is only briefly described here. The LIF reactor was a Pyrex-jacketed cell, internal volume of ∼150 cm^3, housed in a vacuum chamber. The temperature of the reactor was maintained by circulating fluid from a heating or cooling reservoir through the reactor jacket. The temperature of the gas in the LIF reactor was measured with a calibrated thermocouple and was accurate to ±1 K.

OH radicals were produced using two different pulsed laser photolysis sources. H_2O_2 photolysis at 248 nm (KrF excimer laser),

$$H_2O_2 + h\nu \rightarrow OH + OH \quad (3)$$

where the quantum yield for OH production at 248 nm is 2,[15] was used for $k_1(T)$ measurements at temperatures between 240 and 390 K. The H_2O_2 source was not used below 240 K due to condensation of H_2O_2 in the LIF reactor at lower temperatures. The second OH source used was the 193 nm (ArF excimer laser) pulsed photolysis of N_2O in the presence of excess CH_4 in a He bath gas

$$N_2O + h\nu \rightarrow N_2 + O(^1D) \quad (4)$$

$$O(^1D) + CH_4 \rightarrow OH\ (4 \geq v \geq 0) + CH_3 \quad (5a)$$

$$\rightarrow CH_3O + H \quad (5b)$$

$$\rightarrow CH_2O + H_2 \quad (5c)$$

$$\rightarrow O(^3P) + CH_4 \quad (5d)$$

The N_2O/CH_4 source was used for rate coefficient measurements over the temperature range of 210−390 K. The quantum yield for O(^{1}D) production in reaction 4 is unity at 193 nm, and the branching ratios for reactions 5a, 5b, 5c, and 5d are (75 ± 15)%, (20 ± 7)%, (5 ± 5)%, and <1%, respectively.[15] The OH produced in reaction 5a has ∼88% of its population initially in excited vibrational levels.[25] The impact of vibrationally excited OH on the rate coefficient data analysis is discussed later. For the conditions used for the N_2O/CH_4 source in our experiments, >70% of the initially produced O(^{1}D) was converted to OH within 1 μs. Nitric acid photolysis at 248 nm was also tried as a source of OH radicals

$$HNO_3 + h\nu \rightarrow OH + NO_2 \quad (6)$$

However, problems associated with secondary OH generation limited the usefulness of this OH source. A possible interpretation of the secondary OH generation is presented in the Results and Discussion section.

The initial OH radical concentration, $[OH]_0$, was estimated using

$$[OH]_0 = \sigma_\lambda \Phi_\lambda F [\text{precursor}]_{LIF} \quad (7)$$

where σ_λ and Φ_λ are the absorption cross section and OH quantum yield, respectively, for the OH precursor at the photolysis wavelength, λ, F is the photolysis laser fluence (photon cm^{-2} pulse^{-1}), and $[\text{precursor}]_{LIF}$ is the OH precursor concentration in the LIF reactor. The photolysis laser fluence was measured at the exit of the LIF reactor with a calibrated power meter. $[\text{precursor}]_{LIF}$ was determined from flow rates or from the measured pseudo-first-order rate coefficient for the loss of OH in the absence of glyoxal

$$OH + \text{precursor} \rightarrow \text{products} \quad (8)$$

with $k_8(T)$ for CH_4 and H_2O_2 taken from Sander et al.[15] The ranges of $[\text{precursor}]_{LIF}$ used in our experiments were $(8-50) \times 10^{13}$ molecule cm^{-3} for H_2O_2, $(4-10) \times 10^{16}$ molecule cm^{-3} for CH_4, and $(5-20) \times 10^{15}$ molecule cm^{-3} for N_2O. $[OH]_0$ values were in the range of $(9-80) \times 10^{10}$ molecule cm^{-3} during the course of this study.

OH (OD) radicals were excited in the $A^2\Sigma^+ \leftarrow X^2\Pi$ band at 282 nm (287 nm) using the frequency-doubled output of a pulsed Nd:YAG pumped dye laser. The OH (OD) fluorescence signal was detected by a photomultiplier tube (PMT) mounted orthogonal to the photolysis and probe laser beams. A band-pass filter (peak transmission at 310 nm and a 20 nm band-pass, fwhm) mounted in front of the PMT was used to isolate the OH fluorescence. The PMT signal was averaged using a gated charge integrator for 100 laser shots at reaction times between 10 μs to 50 ms.

OH temporal profiles were measured under pseudo-first-order conditions in OH, $[HC(O)C(O)H] \gg [OH]_0$. For the H_2O_2 source, the OH decay followed the expression

$$\ln\left(\frac{[OH]_t}{[OH]_0}\right) = \ln\left(\frac{S_t}{S_0}\right) = -(k_1[HC(O)C(O)H] + k_d)t = -k't \quad (9)$$

where S_t is the OH LIF signal at time t that is proportional to $[OH]_t$, k' and k_d are the pseudo-first-order rate coefficients measured in the presence and absence of glyoxal. k_d represents the loss of OH radicals due to reaction with the OH precursor, buffer gas impurities, and diffusion out of the detection volume. Values of k_d were between 50 and 500 s^{-1}. k' was measured for a range of [HC(O)C(O)H] at each temperature, and $k_1(T)$ was determined from the slope of k' versus [HC(O)C(O)H].

The OH temporal profiles obtained with the N_2O/CH_4 source differed from eq 9 due to the formation of vibrationally excited OH ($4 \geq v \geq 0$) in reaction 5a and its subsequent collisional relaxation to the ground vibrational state.[25,26] In our experiments, only the temporal profile of OH ($v = 0$) was observed. The observed OH temporal profile were well represented by a biexponential expression:

$$S_t = A_1 \exp(-k_q t) + A_2 \exp(-k't) \quad (10)$$

where k_q is an effective first-order rate coefficient for the total loss of vibrationally excited OH ($v > 0$), which includes quenching and reactive loss. Vibrational quenching was primarily by CH_4. [Note: OH ($v = 1$) + He $\rightarrow$ OH ($v = 0$) + He, $k = 1.2 \times 10^{-16}$ cm^3 $molecule^{-1}$ s^{-1} so that under the conditions in our experiments He quenching of vibrationally excited OH is small.] Representing OH vibrational relaxation with an effective first-order rate coefficient is an oversimplification of the actual relaxation mechanism. However, this approximation does not impact the determination of k' due to the separation of time scales for OH vibrational relaxation and OH ($v = 0$) reactive loss. k' was determined by fitting the OH signal versus time to eq 10.

2.1. Materials. He (UHP, 99.999%), N_2 (UHP, >99.99%), O_2 (UHP, >99.99%), CH_4 (>99.97%), N_2O (99.999%), H_2O (>99.99%), and D_2O (>99.9%) were used as supplied. He and N_2 were used as buffer gases in the kinetic measurements when using the H_2O_2 photolysis OH radical source. Concentrated H_2O_2, >95% purity, was prepared by bubbling N_2 for several days through a H_2O_2 sample that was initially at ~60% concentration. Deuterium-enriched H_2O_2/D_2O_2 samples were prepared by adding D_2O to the H_2O_2 sample at the beginning of the purification process. H_2O_2 was added to the LIF reactor by passing a small flow of bath gas, ~1% of the total gas flow, through a bubbler containing the >95% pure liquid H_2O_2. The H_2O_2 reservoir was kept at or below the temperature of the LIF reactor to avoid condensation of H_2O_2 in the LIF reactor.

Glyoxal was obtained commercially in a stable hydrated form (glyoxal trimer-dihydrate, ≥95%). Pure glyoxal monomer was prepared from the solid trimer-dihydrate using the method described by Volkamer et al.[27] Equal masses (~5 g) of glyoxal trimer-dihydrate and solid phosphorus pentoxide (P_2O_5, ≥98%) were mixed and slowly heated under vacuum from 25 to ~160 °C. A small flow of He (~20 STP cm^3 min^{-1}) was passed over the heated sample and through a collection reservoir where the bright yellow pure glyoxal solid was collected at ~ −70 °C. The glyoxal sample was used without further purification. The vapor pressure of the glyoxal sample at 200 K was measured to be ~0.05 Torr (~2×10^{15} molecule cm^{-3}).

2.1.1. Concentration Determination. Glyoxal was introduced into the PLP−LIF gas flow from dilute gas mixtures of glyoxal in He. The mixtures were prepared manometrically in 12 L Pyrex bulbs (darkened to minimize exposure of the sample to room light). Several gas mixtures were prepared over the course of the study with glyoxal mixing ratios of ~0.5% at total pressures of ~1000 Torr (He). The glyoxal/He mixture was added to the PLP−LIF gas flow through a calibrated flow meter. The glyoxal concentration in the LIF reactor, $[\text{glyoxal}]_{LIF}$, was determined using the measured flow rate and the sample mixing ratio in addition to the in situ optical absorption measurements described below.

The $[\text{glyoxal}]_{LIF}$ was determined using in situ UV (at 185 nm) and IR (500−4000 cm^{-1}) absorption. The UV and IR absorptions were also used to check the glyoxal sample purity and for possible loss of glyoxal in the flow through the PLP−LIF apparatus. UV absorption was measured using a Hg pen-ray lamp, a 100 cm long (2.5 cm diameter) absorption cell, a 185 nm narrow band-pass filter, and a solar blind photodiode. Infrared absorption spectra were recorded using a Fourier transform spectrometer between 500 and 4000 cm^{-1} at a spectral resolution of 1 cm^{-1} using 20 coadded scans. A multipass absorption cell (485 cm optical path length, 750 cm^3 total volume, and KBr windows) was used for all IR measurements. UV absorption was measured before the LIF reactor while the infrared absorption spectra were measured either before or after the LIF reactor.

The $[\text{glyoxal}]_{LIF}$ determined from the optical methods were scaled to account for differences in temperature (UV and IR absorption were measured at 296 K), dilution, and pressure between the LIF reactor and absorption cells. The $[\text{glyoxal}]_{LIF}$ was varied over the range of $(9-150) \times 10^{13}$ molecule cm^{-3} during the kinetic measurements. The three methods (flow rates and UV and IR absorption) used to determine $[\text{glyoxal}]_{LIF}$ agreed to within 5% under all measurement conditions used in the determination of $k_1(T)$.

The optical absorption methods were performed independently but do share a common basis in the absorption cross sections used to determine $[\text{glyoxal}]_{LIF}$. The infrared and UV (185 nm) glyoxal absorption cross sections were determined as part of this work. Glyoxal/He mixtures were used to determine absorption cross sections using static fills of the absorption cells and absolute pressure measurements. Absorbances varied linearly with glyoxal concentration over the range of $(0.35-1.2) \times 10^{16}$ molecule cm^{-3} (i.e., obeyed a linear Beer−Lambert relationship) and yielded an absorption cross section, σ_{glyoxal}-(185 nm), of $(3.58 \pm 0.07) \times 10^{-19}$ cm^2 $molecule^{-1}$ (base e). The absorption cross section at the peak of the R-branch, 1740

TABLE 1: Summary of Experimental Conditions and Measured Rate Coefficients for the OH + HC(O)C(O)H (Glyoxal) Reaction, $k_1(T)$, Using Pulsed Laser Photolysis of H_2O_2 as the OH Radical Source

T (K)	P (Torr)	gas	v (cm s^{-1})	$[H_2O_2]$ (10^{14} molecule cm^{-3})	photolysis laser fluence (mJ cm^{-2} pulse^{-1})	$[OH]_0$ (10^{11} molecule cm^{-3})	[HC(O)C(O)H] (10^{14} molecule cm^{-3})	$k_1(T)$ (10^{-12} cm^3 molecule^{-1} s^{-1})[a]
240	104	He	5.6	0.75	8.5	1.4	2.7−14.0	12.3 ± 0.29
247	109	He	12.4	1.3	12.9	3.9	1.8−6.5	11.7 ± 0.29
257	95	He	19.4	1.4	12.1	3.7	0.8−6.1	9.67 ± 0.30
281	104	He	11.9	1.2	8.5	2.3	1.0−7.4	9.61 ± 0.25
281	105	He	12.1	1.5	6.7	2.2	1.1−6.4	9.33 ± 0.18
296	45	He	9.6	1.8	17	6.8	1.16−7.25	9.28 ± 0.37
296	53	He	19.2	1.2	7.9	2.1	1.1−7.8	8.87 ± 0.23
296	97	He	20.1	4.7	2	2.1	1.2−6.4	9.08 ± 0.41
296	97	He	20.3	1.4	6.6	2.1	1.2−7.9	8.63 ± 0.20
296	98	He	7.1	2.0	7.7	3.5	1.19−7.69	8.91 ± 0.22
296	99	He	9.4	1.3	7	2.0	1.9−11.6	8.71 ± 0.41
296	100	He	6.9	2.2	8.1	4.1	1.32−7.74	9.28 ± 0.22
296	103	He	6.8	3.6	6.9	5.6	5.57−15.0	9.13 ± 0.24
296	307	He	5	1.5	4.1	1.4	2.93−23.9	9.44 ± 0.25
296	45	N_2	8.1	1.4	5.1	1.6	2.11−12.1	9.03 ± 0.16
296	46	N_2	8.1	5.2	1.3	1.5	2.37−13.0	9.18 ± 0.24
296	96	N_2	9	2.2	4.1	2.1	1.42−7.09	8.67 ± 0.26
317	102	He	10.1	2.1	8.4	4.0	1.2−6.3	8.70 ± 0.27
342	107	He	8.4	1.4	20.8	6.5	1.7−11.1	8.60 ± 0.27
367	43	He	12.7	2.0	17.7	7.9	1.3−7.7	8.21 ± 0.18
388	111	He	18	1.4	13.4	4.1	0.7−4.6	8.07 ± 0.23
388	304	He	8.5	1.1	6.5	1.5	2.5−11.1	8.15 ± 0.27
391	102	He	9.5	0.89	7.3	1.5	1.7−11.2	8.24 ± 0.25
391	103	He	9.2	1.5	8.2	2.8	1.5−8.6	8.13 ± 0.26
391	104	He	10.5	4.3	3.5	3.4	1.1−7.5	8.18 ± 0.26

[a] The quoted uncertainties are the 2σ precision values obtained using eq 5.

TABLE 2: Summary of Experimental Conditions and Measured Rate Coefficients for the OH + HC(O)C(O)H (Glyoxal) Reaction, $k_1(T)$, Using Pulse Laser Photolysis of N_2O/CH_4 as the OH Radical Source

T (K)	P (Torr, He)	v (cm s^{-1})	$[N_2O]$ (10^{15} molecule cm^{-3})	$[CH_4]$ (10^{16} molecule cm^{-3})	photolysis laser fluence (mJ cm^{-2} pulse^{-1})	$[OH]_0$ (10^{11} molecule cm^{-3})	[HC(O)C(O)H] (10^{14} molecule cm^{-3})	$k_1(T)$ (10^{-12} cm^3 molecule^{-1} s^{-1})[a]
209	51	8.4	5	4	0.326	2	1.5−9.7	14.2 ± 0.32
211	101	7.3	7	5	0.326	2	1.3−9.5	14.0 ± 0.53
221	98	6.8	7	5	0.295	2	2.1−10.6	13.5 ± 0.59
231	100	6.6	6	5	0.282	2	2.4−16.7	12.1 ± 0.53
241	49	13.8	6	5	0.16	0.9	0.7−7.5	11.3 ± 0.72
241	102	6.5	6	5	0.138	0.8	3.1−14.9	12.3 ± 0.24
241	103	6.4	6	5	0.16	0.9	1.6−10.5	11.4 ± 1.03
255	104	6.6	6	6	0.138	0.9	2.6−13.2	10.0 ± 0.86
268	104	6.6	6	6	0.15	0.9	2.8−15.2	9.39 ± 0.87
296	99	6.6	20	5	0.165	4	1.4−11.2	8.55 ± 0.35
296	101	6.8	5	5	0.165	0.9	1.7−10.2	9.14 ± 0.75
296	110	6.3	7	10	0.144	1	3.2−15.8	8.94 ± 0.98
323	107	7.7	8	6	0.139	1	2.6−14.4	8.47 ± 0.33
388	53	8.3	8	4	0.15	1	1.6−9.7	8.12 ± 1.23
388	108	7.5	9	7	0.15	1	1.7−12.8	8.04 ± 0.98

[a] The quoted uncertainties are the 2σ precision values obtained from the fits to eq 5.

cm^{-1}, and the C−H stretch integrated band strength for glyoxal were determined to be $\sigma_{glyoxal}(1740\ cm^{-1}) = (8.11 \pm 0.10) \times 10^{-19}$ cm^2 molecule^{-1} and $S_{glyoxal}(2724-2940\ cm^{-1}) = (1.63 \pm 0.02) \times 10^{-17}$ cm^2 molecule^{-1} cm^{-1}, respectively (base e). The quoted uncertainties in the cross sections are 2σ and are based on the precision in the slope of the linear least-squares analysis of the measured absorbance versus [HC(O)C(O)H]. The IR cross sections measured in this work are in excellent agreement (within 5%) with those reported by Volkamer et al.[27]

Pressures were measured with calibrated 10, 100, or 1000 Torr capacitance manometers. Calibrated electronic mass flow transducers were used to measure gas flows. The gas flow through the reactor was sufficient to flush the gas mixture through the reaction volume between photolysis laser pulses, 10 Hz.

3. Results and Discussion

Rate coefficients for reaction 1, $k_1(T)$, were determined under pseudo-first-order conditions in OH over the temperature range of 210−390 K at pressures between 45 and 300 Torr in He and 50 and 100 Torr in N_2 bath gases. The lowest temperature used in the $k_1(T)$ measurements, 210 K, was established to avoid condensation of glyoxal in the LIF reactor, which was observed at lower temperatures. Tables 1 and 2 summarize the experimental conditions used and the measured $k_1(T)$. $k_1(T)$ was found to be independent of pressure and bath gas over the range of conditions covered in this study.

Figures 2 and 3 show OH temporal profiles that are representative of the data recorded during the $k_1(T)$ measurements. The OH decays were exponential (biexponential when the N_2O/CH_4 OH source was used) for all temperatures and

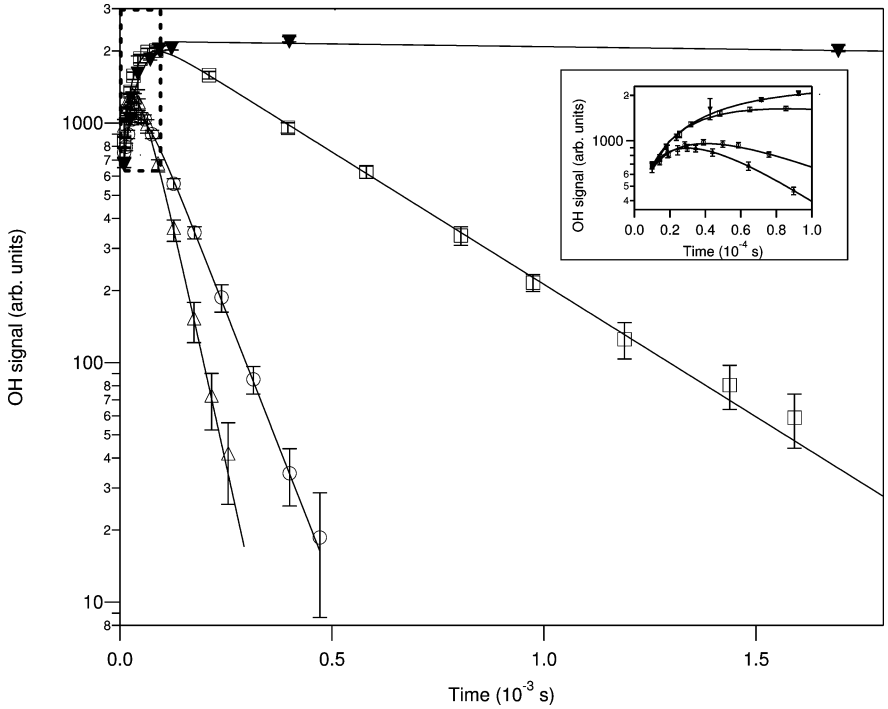

Figure 2. Examples of OH temporal profiles measured using laser-induced fluorescence (LIF) with different glyoxal concentrations: [HC(O)C(O)H] (10^{14} molecule cm^{-3}) = 0 (▼), 2.0 (□), 8.1 (○), and 13 (△). OH profiles were measured at 220 K in 100 Torr of He using 193 nm photolysis of a N_2O/CH_4 mixture as the OH radical source. The error bars on the data points are the 2σ (95% confidence limit) uncertainties from the precision of the OH signal measurement (100 laser shots). The lines are the precision-weighted biexponential fits of the OH profiles to eq 10. The inset shows an expanded view that more clearly shows the rapid growth in ground-state vibrational OH at early times (see text).

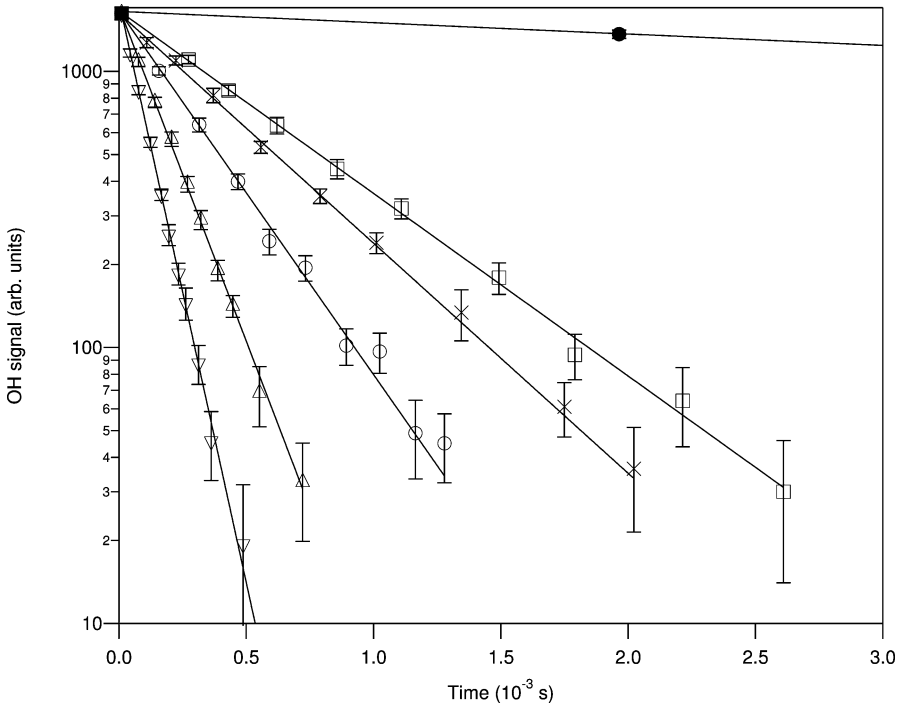

Figure 3. Examples of OH temporal profiles measured using laser-induced fluorescence (LIF) with different glyoxal concentrations: [HC(O)C(O)H] (10^{14} molecule cm^{-3}) = 0 (●), 1.7 (□), 2.2 (×), 3.6 (○), 6.5 (△), and 11.2 (▽). OH profiles were measured at 390 K in 100 Torr of He using H_2O_2 photolysis at 248 nm as the OH source. Profiles measured at other temperatures and pressures were of similar quality. The error bars on the data points are the 2σ (95% confidence limit) uncertainties from the precision of the OH signal measurement (100 laser shots). The lines are the precision-weighted linear least-squares fits of the OH profiles to eq 9.

experimental conditions used. $k_1(T)$ was found to be independent of variations in the experimental conditions such as $[OH]_0$, photolysis laser fluence, pressure, and gas flow velocity, as outlined in Tables 1 and 2. Therefore, we obtained $k_1(T)$ from a simultaneous analysis of all data obtained at a given temperature using eq 9. Figure 4 shows a summary of the ($k' - k_d$) data obtained at 240 and 296 K. The consistency of the data sets indicates the independence of the measurements to variations of the experimental conditions. This analysis yielded $k_1(296\ \text{K}) = (9.15 \pm 0.8) \times 10^{-12}$ cm^3 molecule^{-1} s^{-1} where

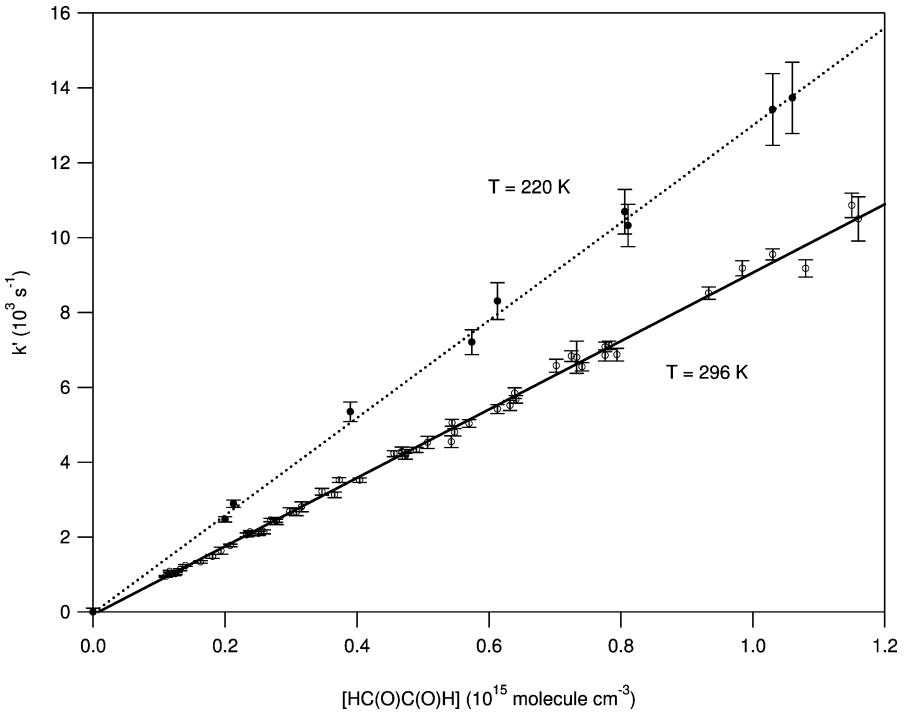

Figure 4. Pseudo-first-order rate coefficient data, ($k' - k_d$), for reaction 1 at 220 and 296 K plotted vs [HC(O)C(O)H]. The error bars are the 2σ (95% confidence limit) uncertainties obtained from the measurement precision. The lines are from the linear least-square analysis of the data, eq 9, and the slopes yield k_1(220 K) and k_1(296 K).

the quoted uncertainties are 2σ (95% confidence level) and include estimated systematic errors (see section 3.1).

The temperature dependence of $k_1(T)$ is shown in Figure 5. $k_1(T)$ shows a negative temperature dependence and deviates slightly from Arrhenius behavior over the range of temperatures studied. A fit of $k_1(T)$ to the form $k(T) = AT^2 \exp(-B/T)$ reproduces the experimental data, within the measurement uncertainty, over the entire range of temperatures included in this study

$$k_1(T) = [(6.6 \pm 0.6) \times 10^{-18}]T^2[\exp([820 \pm 15]/T)] \text{ cm}^3 \text{ molecule}^{-1} \text{ s}^{-1}, \quad T = 210-390 \text{ K} \quad (11)$$

The mechanism for reaction 1 and the non-Arrhenius behavior of $k_1(T)$ are discussed later. For atmospheric modeling purposes, a fit to an Arrhenius expression over the temperature range included in this study that is most relevant to the atmosphere, 210−296 K, yields

$$k_1(T) = (2.8 \pm 0.3) \times 10^{-12} \exp[(340 \pm 30)/T] \text{ cm}^3 \text{ molecule}^{-1} \text{ s}^{-1}, \quad T = 210-296 \text{ K} \quad (12)$$

which reproduces the measured $k_1(T)$ very well and is included in Figure 5 for comparison.

Rate coefficients, $k_{1d}(T)$, for the reaction

$$\text{OD} + \text{HC(O)C(O)H} \rightarrow \text{HOD} + \text{HC(O)C(O)} \quad (1d)$$

were measured under pseudo-first-order conditions in OD at 296, 350, and 390 K at total pressures of 45 and 100 Torr He. OD radicals were produced by the 248 nm pulsed laser photolysis of D_2O_2 (using a deuterium enriched H_2O_2 sample). The OD temporal profiles were exponential for all experimental conditions, i.e., obeyed eq 9. Table 3 summarizes the experimental conditions used and the measured $k_{1d}(T)$ values. A fit to a linearized Arrhenius expression yields $k_{1d}(T) = (3.7 \pm 0.5) \times 10^{-12} \exp[(285 \pm 40)/T]$ cm^3 molecule^{-1} s^{-1} and is consistent with a small secondary kinetic isotope effect ($0.9 < k_1/k_{1d} < 1$). The measured $k_{1d}(T)$ values are also included in Figure 5.

3.1. Error Analysis. The accuracy of $k_1(T)$ obtained in this work was dependent on the precision of the measurements, the uncertainty in the determination of $[\text{glyoxal}]_{\text{LIF}}$, and possible systematic errors. The kinetic measurements are of high precision and contribute <5% to the uncertainty in $k_1(T)$. We estimate the systematic uncertainties in the experimental parameters to be relatively small: ±1% in total pressure, ±2% in flow rate, and <1% in temperature. The largest source of uncertainty (systematic) in the present study lies in the determination of $[\text{glyoxal}]_{\text{LIF}}$. The uncertainty in the UV and infrared absorption cross sections of glyoxal determined in this work are estimated to be ∼5%. Absorption measurements made before and after the reactor were in excellent agreement, within 2%, at all temperatures, implying no measurable loss of glyoxal in the LIF reactor. In addition, no evidence for glyoxal dimerization[28] at low temperatures was observed, i.e., the measured pseudo-first-order rate coefficients were linear with respect to the glyoxal concentration as shown in Figure 4. At elevated temperatures, no thermal decomposition of the glyoxal was observed.

The possible loss of glyoxal from the gas flow due to homogeneous or heterogeneous reaction with H_2O vapor was tested experimentally and found to be insignificant under our normally dry measurement conditions, $[H_2O] < 10^{14}$ molecule cm^{-3}. However, the addition of 1.5×10^{16} molecule cm^{-3} of H_2O to the LIF reactor (296 K) lead to a measurable glyoxal loss; a 25% loss was observed between the UV and IR absorption cells. In summary, the $[\text{glyoxal}]_{\text{LIF}}$ determined from the gas flow and UV and IR absorption measurements are accurate to within ±6% for all the experimental conditions used in the determination of $k_1(T)$.

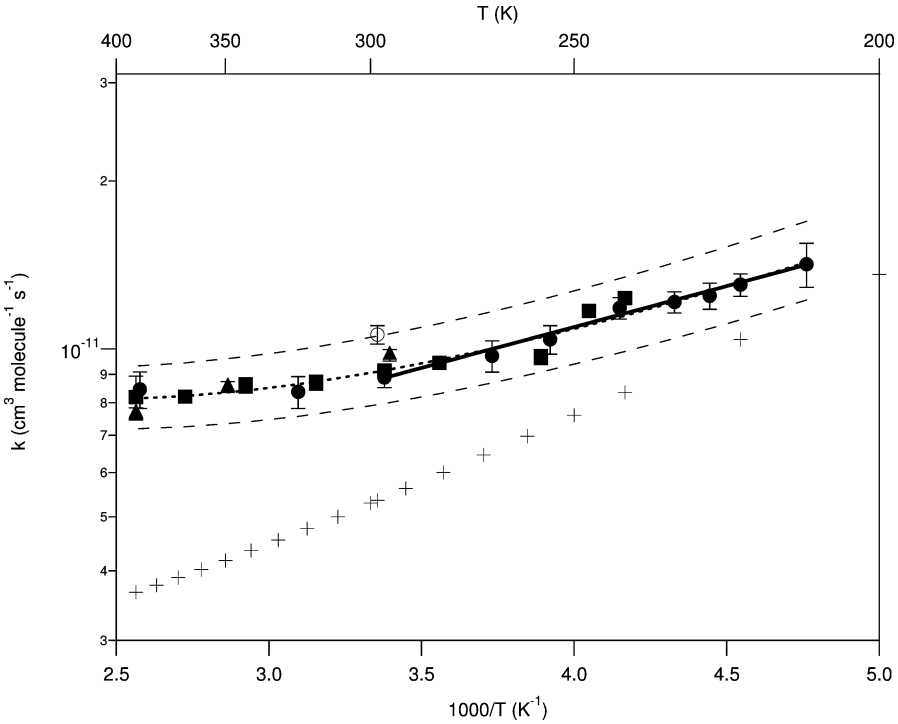

Figure 5. Temperature dependence for the OH + glyoxal reaction rate coefficient, $k_1(T)$, and comparison with previously reported values. The data from this work are given as solid symbols (■, H_2O_2 source; ●, N_2O/CH_4 source; ▲, OD + glyoxal reaction, D_2O_2 source). The error bars are the 2σ precision values (95% confidence limit) from the analysis of the data using eq 9 with the exception of the data points at the temperature extremes that also include estimated systematic errors (see text for error analysis). A fit to all of the OH + glyoxal data from our work (dotted line) yields $k_1(T) = [(6.6 \pm 0.6) \times 10^{-18}]T^2[\exp([820 \pm 15]/T)]$ cm^3 molecule^{-1} s^{-1} for the temperature range of 210−390 K. A fit to an Arrhenius equation (solid line), over the temperature range of 210−296 K, yields $k_1(T) = (2.8 \pm 0.3) \times 10^{-12} \exp[(340 \pm 30)/T]$ cm^3 molecule^{-1} s^{-1}. The dashed lines are the 2σ (including estimated systematic errors) range of rate coefficients from the global fit. The room-temperature measurement of Plum et al. (ref 12) (○) and the theoretical results of Galano et al. (ref 23) (+) are included for comparison.

TABLE 3: Summary of Experimental Conditions and Measured Rate Coefficients for the OD + HC(O)C(O)H (Glyoxal) Reaction, $k_{1d}(T)$

T (K)	P (Torr, He)	v (cm s^{-1})	$[D_2O_2]$ (10^{14} molecule cm^{-3})	photolysis laser fluence (mJ cm^{-2} pulse^{-1})	$[OD]_0$ (10^{11} molecule cm^{-3})	[HC(O)C(O)H] (10^{14} molecule cm^{-3})	$k_{1d}(T)$[b] (10^{-12} cm^3 molecule^{-1} s^{-1})[a]
293	107	6.0	1.1	13.5	3	1.5−10.5	9.68 ± 0.19
296	45	6.5	1.5	9.9	3	3.1−8.9	9.37 ± 0.27
349	101	6.0	1.6	12.8	5	4.6−12.4	8.54 ± 0.19
390	45	6.2	1.4	16.1	5	2.7−9.0	7.67 ± 0.17

[a] The quoted uncertainties are the 2σ precision values obtained from the fits to equation 5.

Impurities in the glyoxal sample represent another potential source of systematic error in the determination of $k_1(T)$. The most likely reactive impurities originate from the sample preparation and include CO and HC(O)H. The purity and stability of the glyoxal/He mixtures were checked periodically via infrared absorption spectroscopy. Infrared absorption spectra showed no loss of glyoxal from the initially prepared mixture or formation of any degradation products for samples kept for up to 3 weeks. The most reactive of the above impurities with OH is HC(O)H, which has a temperature-independent rate coefficient of 9.0×10^{-12} cm^3 molecule^{-1} s^{-1}.[15] Based on our infrared measurements, we estimate the HC(O)H impurity to be <1%, which would not significantly affect the $k_1(T)$ measurement. In addition, rate coefficient measurements performed using the same glyoxal/He mixture over a 3 week period yielded identical $k_1(T)$ values. Finally, experiments performed using glyoxal samples prepared in separate synthesis also yielded identical rate coefficient results.

Nitric acid was used as a source of OH in a few test experiments. The OH temporal profiles measured were nonexponential and consistent with OH production due to secondary chemistry. We attribute the formation of OH under these conditions to the following sequence of reactions

$$HCO + NO_2 \rightarrow H + CO_2 + NO \quad (13)$$

$$H + NO_2 \rightarrow OH + NO \quad (14)$$

where $k_{13}(296\ \text{K}) = 3.0 \times 10^{-11}$ cm^3 molecule^{-1} s^{-1},[29] and $k_{14}(296\ \text{K}) = 1.4 \times 10^{-10}$ cm^3 molecule^{-1} s^{-1}.[15] NO_2 was an impurity in the HNO_3 sample, and the HCO radical was produced as a glyoxal reaction product. Based on our infrared absorption measurements, we estimate a ~5% NO_2 impurity in the HNO_3 sample used. This corresponds to $[NO_2]_{LIF} = \sim 1 \times 10^{14}$ molecule cm^{-3} and a first-order rate coefficient for OH formation of ~3000 s^{-1}. Due to uncertainties in the interpretation of this chemistry and its possible impact on $k_1(T)$, we have

TABLE 4: Comparison of Rate Coefficients for the OH Reaction with Several Small Aldehydes

molecule		k(296 K) (10^{-12} cm^3 molecule^{-1} s^{-1})	ref	SAR k(296 K) (10^{-12} cm^3 molecule^{-1} s^{-1})[a]
glyoxal	HC(O)C(O)H	9.15 ± 0.8	this work	25.3
formaldehyde	HC(O)H	$8.5 +1.7/-1.4$	16	8.1
acetaldehyde	$CH_3C(O)H$	15 ± 3	16	17
methylglyoxal	$CH_3C(O)C(O)$ H	13.2 ± 3	31	13
glycolaldehyde	$HOCH_2C(O)H$	8.0 ± 0.8	32	23.4

[a] Rate coefficients calculated using the structure−activity relationships (SAR) reported by Kwok and Atkinson (ref 14).

not included measurements using the HNO_3 source in the determination of $k_1(T)$.

The overall uncertainty in $k_1(T)$ including the propagation of possible systematic errors is estimated to be ±9% at the 2σ level. The estimated systematic uncertainty is included in the pre-exponential factors in eqs 10 and 11, whereas the uncertainties in the exponential terms were taken from the precision of the least-squares analysis.

3.2. Comparison with Previous Studies. Plum et al. reported[12,16] $k_1(298 \pm 2\ \text{K}) = (11.5 \pm 0.4) \times 10^{-12}$ cm^3 molecule^{-1} s^{-1} from a relative rate study using the OH + cyclohexane reaction as the reference with $k_{\text{cyclohexane}} = 7.57 \times 10^{-12}$ cm^3 molecule^{-1} s^{-1}. Since the Plum et al. study was completed, the recommended rate coefficient for the OH + cyclohexane reaction has been revised, $k_{\text{cyclohexane}} = 2.88 \times 10^{-17} T^2 \exp(309/T)$ cm^3 molecule^{-1} s^{-1},[30] which results in a decrease in their $k_1(298\ \text{K})$ value to $(10.9 \pm 0.4) \times 10^{-12}$ cm^3 molecule^{-1} s^{-1}. Our $k_1(296\ \text{K})$ value of $(9.15 \pm 0.8) \times 10^{-12}$ cm^3 molecule^{-1} s^{-1} is in reasonable agreement with the Plum et al. value, although 15% lower than their revised value. The source of the small discrepancy between the two values is not clear. However, we should point out that the uncertainty in the Plum et al. rate coefficient is based solely on the precision of their relative rate measurement and may be somewhat underestimated. There are no experimental values available to compare with our measured temperature dependence for reaction 1, $k_1(T)$. The theoretically predicted temperature dependence for k_1 is, however, similar to that measured in this work as discussed further below.

The present results can also be compared with OH rate coefficients for other aldehydes. Table 4 lists rate coefficient data for formaldehyde, acetaldehyde, glycolaldehyde, and methylglyoxal and includes the room-temperature OH rate coefficients calculated using the SAR for comparison.[14] In general, the SAR estimation method works very well, and Table 4 shows that the agreement between the SAR and experimental values is within 15% for formaldehyde, acetaldehyde, and methylglyoxal. However, the experimental and SAR values for glyoxal and glycolaldehyde differ by nearly a factor of 3. The large differences found for the glyoxal and glycolaldehyde reactions imply that their reaction mechanisms differ from that of the other aldehydes.

Figure 5 shows that $k_1(T)$ exhibits a non-Arrhenius temperature-dependent behavior. A non-Arrhenius behavior has been observed for other carbonyl containing compounds, including formaldehyde (HC(O)H),[22] formic acid (HC(O)OH),[33] acetic acid ($CH_3C(O)OH$),[34] and acetone ($CH_3C(O)CH_3$),[35] and is generally attributed to the formation of a hydrogen-bonded prereactive complex.[20,21] The shape and magnitude of the temperature-dependent behavior in each of these cases is different and depends on the specific details of the reaction potential energy surface, including the stabilization energy of the reaction complex, the transition state structure and energy, and tunneling probabilities.

The mechanism for the OH + glyoxal reaction has been studied theoretically using quantum chemistry and canonical variational transition state theory including small curvature tunneling by Galano et al.[23] to determine $k_1(T)$. The reaction mechanism includes the formation of a hydrogen-bonded adduct as a reaction intermediate

$$\text{OH} + \text{HC(O)C(O)H} \leftrightarrow \text{HC(O}-\text{HO)C(O)H} \qquad (15)$$

where the stabilization energy for the adduct is ~2.5 kcal mol^{-1}. Formation of reaction products proceeds by abstraction of the H atom from the adjacent C atom. The experimentally determined pressure independence of reaction 1 is consistent with such a low adduct stabilization energy. Similar pressure-independent behavior has been observed for the OH + acetone reaction, for which the hydrogen-bonded adduct has a stabilization energy of ~5 kcal mol^{-1}.[35] The calculated $k_1(296\ \text{K})$ value of 5.35×10^{-12} cm^3 molecule^{-1} s^{-1} is ~40% lower than our experimentally observed value. The calculations yielded a negative non-Arrhenius temperature dependence, which is also in qualitative agreement with our experimental results. However, the calculated temperature dependence is significantly greater than observed in our measurements as shown in Figure 5. The source of the discrepancies between the theoretical predictions and our experimental results are, however, not easy to identify. The energies of the adduct and the transition state relative to the reactants were calculated to be −2.5 kcal mol^{-1} and −1.3 kcal mol^{-1}, respectively,[23] where the uncertainty in these values is expected to be ±1 kcal mol^{-1}.[36] Due to the small energy differences between the adduct and transition state, the structures and exact energies of the adduct and transition state can critically affect the calculated rate coefficients. It is also important to note that the study by Galano et al.[23] assumes that the hydrogen-bonded adduct is collisionally stabilized (i.e., has reached thermal equilibrium). The works of Klippenstein and co-workers[37,38] have shown that such an assumption may not be correct and a more thorough theoretical treatment may be required to accurately predict the reaction rate coefficient.

Despite discrepancies in the magnitude of the theoretical values reported by Galano et al.[23] and the experimental rate coefficient data obtained in this work, the qualitative agreement suggests that the proposed reaction mechanism is generally correct. Our experimental results, including our OD + glyoxal rate coefficients, should therefore provide the basis for further more refined computational studies. Additional details regarding the reaction mechanism could also be obtained from the OH + glyoxal-d_2 rate coefficient, which is presently not known.

3.3. Secondary Chemistry and the Formation of OH Radicals. It was discovered, during the course of our work, that the addition of O_2 to the reaction mixture resulted in the formation of OH in the chemistry following reaction 1. OH formation was observed indirectly through a systematically

lower $k_1(T)$ measured in the presence of O_2 and nonexponential decays of OH at longer measurement times. The observed change in $k_1(T)$ increased with decreasing temperature and increasing $[O_2]$. For the limited range of conditions used in these experiments, the largest change in $k_1(T)$ observed was ~30%. The chemistry leading to the formation of OH radicals is not known, but there are only a few reactive species expected to be present following reaction 1. A primary radical product in reaction 1 is HC(O)C(O). The formation of OH as observed in our experiments is, however, not consistent with the currently accepted chemistry for the HC(O)C(O) radical.[39,40] In the presence of O_2, the HC(O)C(O) radical is expected to either thermally dissociate

$$HC(O)C(O) \rightarrow HCO + CO \quad (16)$$

where $k_{16}(T) = 1.4 \times 10^{12} \exp(-3160/T)\ s^{-1}$ at 700 Torr; $k_{16}(296\ K) = 3.2 \times 10^7\ s^{-1}$,[40] or react with O_2, by either hydrogen abstraction or addition,

$$HC(O)C(O) + O_2 \rightarrow HO_2 + 2CO \quad (17a)$$

$$HC(O)C(O) + O_2 + M \rightarrow HC(O)C(O)O_2^* + M \quad (17b)$$

where $HC(O)COO_2^*$ represents an energetically excited peroxy radical. k_{17} is not known but is expected to be on the order of 10^{-11} cm^3 molecule^{-1} s^{-1}.[40] The HCO radical formed in reaction 16 will rapidly react with the O_2 that is present in large excess to produce HO_2

$$HCO + O_2 \rightarrow HO_2 + CO \quad (18)$$

The rate coefficient for the reaction of HO_2 with glyoxal is slow, 5×10^{-16} cm^3 molecule^{-1} s^{-1},[39] and therefore not important on the time scale of our measurements. In addition, the radical concentrations in our experiments are sufficiently low that radical−radical reactions will also not be significant on the time scale of our measurements. We speculate that OH could be formed from $HC(O)C(O)O_2^*$ prior to its collisional stabilization via a mechanism analogous to that observed for the $CH_3CO + O_2 + M$ reaction.[41,42] Additional data are needed to identify and quantify the actual source of the observed OH production; however, it is important to note that OH production from secondary chemistry in the presence of O_2 did not affect our determination of $k_1(T)$ or the relative rate study of Plum et al.[12] In the relative rate study, the relative loss rates of glyoxal and cyclohexane by reaction with OH would remain unchanged. In our work, there was no experimental evidence for secondary formation of OH that would influence our determination of $k_1(T)$ in the absence of O_2. The consistency of our measured rate coefficient for the OD + glyoxal reaction, k_{1d}, with k_1, $k_{1d}(296\ K) = 1.07\ k_1(296\ K)$, also implies that OH generation in the absence of O_2 did not impact our determination of $k_1(T)$. Thus, secondary OH formation is not the source of the small discrepancy in $k_1(296\ K)$ from these two studies.

4. Atmospheric Implications

A goal of the present study was to obtain an improved characterization of the glyoxal atmospheric lifetime, in particular with respect to reaction with OH. Since glyoxal is an important source of HO_x in the troposphere, quantifying its HO_x production is also important. Other than the OH reaction, glyoxal is known to be removed from the atmosphere by UV photolysis[8,43] and heterogeneously via reactive uptake.[9−11] Under typical daylight conditions, UV photolysis is expected to be the primary gas-phase loss process for glyoxal.[12,43] Nevertheless, it is important to quantify all loss processes for glyoxal that occur in the atmosphere.

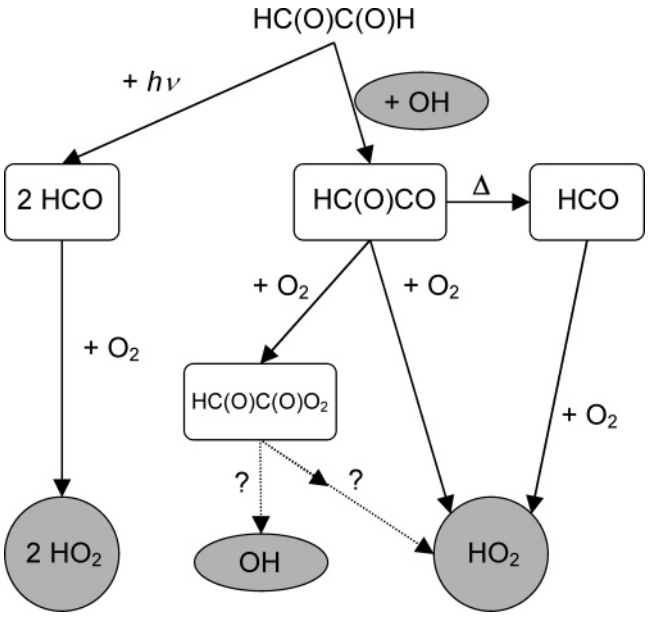

Figure 6. Simplified atmospheric degradation scheme for glyoxal showing its loss via UV photolysis, leading to a net production of HO_x, and the OH reaction with no net HO_x production. The branching ratio for the loss of glyoxal favors UV photolysis over OH reaction under typical atmospheric conditions. However, the photolysis rate is pressure and wavelength dependent, and thus the branching ratio for loss of glyoxal will depend on altitude, solar zenith angle, and cloud coverage. The fate of the $HC(O)C(O)O_2$ radical is not currently understood, but experimental evidence from this work and previous studies (refs 39 and 40) suggests it will lead to the formation of HO_x under atmospheric conditions.

HO_x production from glyoxal depends on the branching between its loss by UV photolysis and reaction with OH as outlined in Figure 6. UV photolysis of glyoxal leads to the formation of 2 HCO radicals under atmospheric conditions,[43] which in turn yields a net production of two HO_2 radicals. The OH + glyoxal reaction, on the other hand, leads to the formation of an unstable carbonyl radical, HC(O)C(O). As discussed earlier, HC(O)C(O) will thermally decompose or react with O_2 to form $HC(O)C(O)O_2$. The fate of the peroxy radical, $HC(O)C(O)O_2$, is uncertain, but it is expected to yield a HO_x radical. Therefore, the OH + glyoxal reaction overall yields no net HO_x radical formation. In other words, two HO_x radicals are produced in the UV photolysis of glyoxal while no net HO_x radical production occurs for OH reactive loss. On the basis of our $k_1(T)$ measurements, a $k_1(296\ K)$ value that is ~15% lower than currently recommended,[15,16] the loss of glyoxal via UV photolysis and its HO_x production are underestimated in current atmospheric models. Including the temperature dependence for the OH + glyoxal reaction will, however, partially offset the underestimation.

Acknowledgment. This work was supported in part by NOAA's Health of the Atmosphere and Air Quality Programs.

References and Notes

(1) Carter, W. P. L.; Atkinson, R. *Int. J. Chem. Kinet.* **1996**, *28*, 497.
(2) Ham, J. E.; Proper, S. P.; Wells, J. R. *Atmos. Environ.* **2006**, *40*, 726.
(3) Magneron, I.; Thevenet, R.; Mellouki, A.; Le Bras, G.; Moortgat, G. K.; Wirtz, K. *J. Phys. Chem. A* **2002**, *106*, 2526.

(4) Nunes, F. M. N.; Veloso, M. C. C.; Pereira, P.; de Andrade, J. B. *Atmos. Environ.* **2005**, *39*, 7715.
(5) Volkamer, R.; Platt, U.; Wirtz, K. *J. Phys. Chem. A* **2001**, *105*, 7865.
(6) Wittrock, F.; Richter, A.; Oetjen, H.; Burrows, J. P.; Kanakidou, M.; Myriokefalitakis, S.; Volkamer, R.; Beirle, S.; Platt, U.; Wagner, T. *Geophys. Res. Lett.* **2006**, *33*, L16804.
(7) Volkamer, R.; Molina, L. T.; Molina, M. J.; Shirley, T.; Brune, W. H. *Geophys. Res. Lett.* **2005**, *32*, L08806.
(8) Atkinson, R. *Atmos. Environ.* **2000**, *34*, 2063.
(9) Hastings, W. P.; Koehler, C. A.; Bailey, E. L.; De Haan, D. O. *Environ. Sci. Technol.* **2005**, *39*, 8728.
(10) Kroll, J. H.; Ng, N. L.; Murphy, S. M.; Varutbangkul, V.; Flagan, R. C.; Seinfeld, J. H. *J. Geophys. Res., [Atmos.]* **2005**, *110*, D23207.
(11) Liggio, J.; Li, S. M.; McLaren, R. *J. Geophys. Res., [Atmos.]* **2005**, *110*, D10304.
(12) Plum, C. N.; Sanhueza, E.; Atkinson, R.; Carter, W. P. L.; Pitts, J. N. *Environ. Sci. Technol.* **1983**, *17*, 479.
(13) Chen, Y. Q.; Zhu, L. *J. Phys. Chem. A* **2003**, *107*, 4643.
(14) Kwok, E. S. C.; Atkinson, R. *Atmos. Environ.* **1995**, *29*, 1685.
(15) Sander, S. P.; Finlayson-Pitts, B. J.; Friedl, R. R.; Golden, D. M.; Huie, R. E.; Keller-Rudek, H.; Kolb, C. E.; Kurylo, M. J.; Molina, M. J.; Moortgat, G. K.; Orkin, V. L.; Ravishankara, A. R.; Wine, P. H. *Chemical Kinetics and Photochemical Data for Use in Atmospheric Studies, Evaluation Number 15*; JPL Publication 02-25; NASA Jet Propulsion Laboratory, California Institute of Technology: Pasadena, CA, 2006.
(16) Atkinson, R.; Baulch, D. L.; Cox, R. A.; Crowley, J. N.; Hampson, R. F.; Hynes, R. G.; Jenkin, M. E.; Rossi, M. J.; Troe, J. *Atmos. Chem. Phys.* **2006**, *6*, 3625.
(17) Butkovskaya, N. I.; Pouvesle, N.; Kukui, A.; Le Bra, G. *J. Phys. Chem. A* **2006**, *110*, 13492.
(18) Cameron, M.; Sivakumaran, V.; Dillon, T. J.; Crowley, J. N. *Phys. Chem. Chem. Phys.* **2002**, *4*, 3628.
(19) Sivakumaran, V.; Holscher, D.; Dillon, T. J.; Crowley, J. N. *Phys. Chem. Chem. Phys.* **2003**, *5*, 4821.
(20) Smith, I. W. M.; Ravishankara, A. R. *J. Phys. Chem. A* **2002**, *106*, 4798.
(21) Alvarez-Idaboy, J. R.; Mora-Diez, N.; Boyd, R. J.; Vivier-Bunge, A. *J. Am. Chem. Soc.* **2001**, *123*, 2018.
(22) D'Anna, B.; Bakken, V.; Beukes, J. A.; Nielsen, C. J.; Brudnik, K.; Jodkowski, J. T. *Phys. Chem. Chem. Phys.* **2003**, *5*, 1790.
(23) Galano, A.; Alvarez-Idaboy, J. R.; Ruiz-Santoyo, M. E.; Vivier-Bunge, A. *ChemPhysChem* **2004**, *5*, 1379.
(24) Vaghjiani, G. L.; Ravishankara, A. R. *J. Phys. Chem.* **1989**, *93*, 1948.
(25) Cheskis, S. G.; Iogansen, A. A.; Kulakov, P. V.; Razuvaev, I. Y.; Sarkisov, O. M.; Titov, A. A. *Chem. Phys. Lett.* **1989**, *155*, 37.
(26) Ausfelder, F.; Hippler, H.; Striebel, F. *Z. Phys. Chem.* **2000**, *214*, 403.
(27) Volkamer, R.; Spietz, P.; Burrows, J.; Platt, U. *J. Photochem. Photobiol., A* **2005**, *172*, 35.
(28) Derose, P.; Dai, H. L.; Cheng, P. Y. *Chem. Phys. Lett.* **1994**, *220*, 207.
(29) Guo, Y. L.; Smith, S. C.; Moore, C. B.; Melius, C. F. *J. Phys. Chem.* **1995**, *99*, 7473.
(30) Atkinson, R. *J. Phys. Chem. Ref. Data* **1997**, *26*, 215.
(31) Tyndall, G. S.; Staffelback, T. A.; Orlando, J. J.; Calvert, J. G. *Int. J. Chem. Kinet.* **1995**, *27*, 1009.
(32) Karunanandan, R.; Holscher, D.; Dillon, T. J.; Horowitz, A.; Crowley, J. N.; Vereecken, L.; Peeters, J. *J. Phys. Chem. A* **2007**, *111*, 897.
(33) Singleton, D. L.; Paraskevopoulos, G.; Irwin, R. S.; Jolly, G. S.; McKenney, D. J. *J. Am. Chem. Soc.* **1988**, *110*, 7786.
(34) Singleton, D. L.; Paraskevopoulos, G.; Irwin, R. S. *J. Am. Chem. Soc.* **1989**, *111*, 5248.
(35) Talukdar, R. K.; Gierczak, T.; McCabe, D. C.; Ravishankara, A. R. *J. Phys. Chem. A* **2003**, *107*, 5021.
(36) Lynch, B. J.; Truhlar, D. G. *J. Phys. Chem. A* **2001**, *105*, 2936.
(37) Georgievskii, Y.; Klippenstein, S. J. *J. Phys. Chem. A* **2007**, *111*, 3802.
(38) Greenwald, E. E.; North, S. W.; Georgievskii, Y.; Klippenstein, S. J. *J. Phys. Chem. A* **2005**, *109*, 6031.
(39) Niki, H.; Maker, P. D.; Savage, C. M.; Breitenbach, L. P. *Int. J. Chem. Kinet.* **1985**, *17*, 547.
(40) Orlando, J. J.; Tyndall, G. S. *Int. J. Chem. Kinet.* **2001**, *33*, 149.
(41) Blitz, M. A.; Heard, D. E.; Pilling, M. J. *Chem. Phys. Lett.* **2002**, *365*, 374.
(42) Tyndall, G. S.; Orlando, J. J.; Wallington, T. J.; Hurley, M. D. *Int. J. Chem. Kinet.* **1997**, *29*, 655.
(43) Tadic, J.; Moortgat, G. K.; Wirtz, K. *J. Photochem. Photobiol., A* **2006**, *177*, 116.